Accepted version of Electrochim. Acta, 82 (2012) 550-557. doi: 10.1016/j.electacta.2012.04.150



# Kinetic study of CO oxidation on clean and oxidized Pt

P. K. Dahlstrøm[a], David A. Harrington[*,b], F. Seland[**,a]

[a] *Department of Materials Science and Engineering, Norwegian University of Science and Technology, 7491 Trondheim, Norway*
[b] *Department of Chemistry, University of Victoria, Victoria, British Columbia, V8W 3V6, Canada.*

**Abstract**

Bulk CO oxidation on smooth polycrystalline platinum was studied with a rotating disk electrode and cyclic voltammetry in CO-saturated 0.5 M sulfuric acid. The reaction rate was modelled with differential equations. The modelling goal was to build a model that reproduces the experimental current-potential characteristics, with special attention to the platinum oxide region. Two different models were tested: one containing conventional chemical and electrochemical reaction steps, and one built around an empirical equation describing the rate of platinum oxide formation and reduction. The latter model produced good fits to the experimental results. Both models showed that CO oxidation in the platinum oxide range proceeds via direct reaction between an adsorbed species such as PtOH and dissolved CO.

*Key words:* CO oxidation, platinum, oxide, RDE, kinetic model

## 1. Introduction

An understanding of the mechanism of CO oxidation has relevance to direct liquid fuel cells using simple organic molecules as fuels, since adsorbed CO is a poisoning intemediate in the electrooxidation reactions. However, CO oxidation also has intrinsic interest as a model system that is simple and

*Principal corresponding author. Tel.: +1-250-7217166, Fax: +1-250-7217147
**Corresponding author. Tel.: +47 73 59 40 42, Fax: +47 73 55 02 03
*Email addresses:* per.dahlstrom@material.ntnu.no (P. K. Dahlstrøm), dharr@uvic.ca (David A. Harrington), frodesel@material.ntnu.no (F. Seland)

is accessible to spectroscopic and computational studies. Oxidation of CO on platinum is a well-studied system in the literature (reviewed here [1–6]), both as oxidation of an adsorbed monolayer without CO in the solution and as continuous oxidation with CO present in the solution. The latter normally involves means to control the mass-transfer to the electrode, like the rotating disk electrode [7, 8], wall-jet electrode [9, 10], or flow cell [11]. Many CO oxidation studies are performed, partially or completely, by modelling. Different modelling methods have been applied by different research groups: dynamic Monte Carlo simulations, density functional theory (DFT), or solving a set of differential equations based on reaction kinetics [12–16].

Oxidation of CO is normally assumed to follow the Langmuir-Hinshelwood mechanism, where adsorbed CO reacts with an adsorbed oxygen-containing species to form $CO_2$. The nature of the oxygen-containing species is still not fully known, but is usually assumed to be OH(ads), formed by electrochemical adsorption of water. An important factor in the CO oxidation kinetics is the surface diffusion of adsorbed CO. Without sufficiently fast surface diffusion, the normal assumption of the mean-field approximation fails [17]. Evidence in the literature seems to both support and reject the mean-field approximation for adsorbed CO on platinum. Becdelièvre et al. [18] conclude that CO is immobile on a platinum surface, while Koper et al. [19] and Housmans et al. [20], by comparing experimental results with Monte Carlo simulation of a simple Langmuir-Hinshelwood mechanism with fast and slow surface diffusion, conclude that their modelling results with fast surface diffusion better resemble the experimental results. Others have also reached this conclusion [21].

In experimental studies, only a few have explored CO oxidation in the potential range of platinum oxide formation. Most papers reporting cyclic voltammetry of platinum in CO-saturated electrolyte stop the sweep soon after the CO oxidation peak [22–24]. The upper reversible potential is thus typically 1.0-1.1 V. A few exceptions exist though: both Mayrhofer [3] and Stalnionis [9] report studies of bulk CO oxidation with an electrode potential up to approximately 1.5 V.

When it comes to the modelling studies, a limited number of papers have been found that model CO oxidation in the potential range of full coverage of platinum oxide, but several papers report modelling of CO oxidation with potentials up to approximately 1.0-1.1 V. Saravanan et al. [12, 25] have studied the effect of varying rate parameters, adsorption of anions, and CO surface diffusion on CO oxidation with Monte Carlo simulations. Bonnefont

et al. [26, 27] studied the formation of spatial patterns during bulk CO oxidation both experimentally and by a mathematical model. Both these groups employed a simple model based on the Langmuir-Hinshelwood mechanism. A maximum coverage of adsorbed OH was assumed to avoid problems with OH blocking all the active sites at potentials higher than the oxidation peak. Orts et al. [13] used Monte Carlo simulations to explain the appearance of two CO oxidation peaks in the experimental voltammograms at some CO coverages. They concluded that different arrangements of the adsorbed CO at low and high coverage result in a CO adlayer that is either easy or hard to oxidize, respectively. Azevedo et al. [28] built an impedance model based on the Langmuir-Hinshelwood mechanism, which fitted well to experimental data. The papers by Janik et al. [29, 30] are unusual in dealing with oxidation above 1.1 V; DFT calculations show that the activation barrier for reaction between adsorbed CO with adsorbed OH is significantly smaller than for the reaction between adsorbed CO and adsorbed O in the potential range 0-1.6 V. Thus, they concluded that the oxygen-containing species is PtOH. Narayanasamy and Anderson [31] used DFT to calculate the activation energies of different reaction pathways from CO(ads) to $CO_2$ and concluded that CO(ads) reacts with PtOH.

In this work, bulk CO oxidation on smooth platinum is studied experimentally with a rotating disk electrode and by modelling. The modelling goal was to build a model that predicts the current-potential behavior of bulk CO-oxidation not only at the main oxidation peak but also well into the platinum oxide range. The upper potential limit used was 1.6 V. This target was pursued by assuming a set of elementary chemical and electrochemical reaction steps, building a set of differential equations based on the rate equations, and calculating the current-potential characteristics by solving this equation set. Two different approaches are used: one model contains only elementary electrochemical reactions and another uses an empirical equation to describe the platinum oxide growth rate. The second approach predicts the current-potential behavior well, both for the positive-going and the negative-going scans.

## 2. Experimental

The experiments used a standard three-electrode system with a Pine Research Instruments polycrystalline smooth platinum rotating disk electrode as working electrode, a Pt wire counter electrode and a reversible hydro-

gen reference electrode (RHE). All potentials are referred to this reference electrode.

All glassware was cleaned by overnight immersion in hot concentrated sulfuric acid followed by subsequent immersion and rinsing in Milli-Q water. In all experiments, 0.5 M sulfuric acid was used as electrolyte. Oxygen was removed by Ar-bubbling prior to the experiments. Before the experiments were performed, the working electrode was cycled at 100 mV $s^{-1}$ between 0.05 and 1.60 V for 1 hour. Then, the electrode was characterized with cyclic voltammetry at different sweep rates. All currents were normalized to the electrochemically active surface area, by integrating the charge under the hydrogen adsorption/desorption peaks and dividing by 220 $\mu$C $cm^{-2}$. To perform experiments in CO-saturated electrolyte, Ar-bubbling was replaced with CO-bubbling, and the electrode was cycled for another hour at 100 mV $s^{-1}$ within the same potential limits.

Bulk CO oxidation was characterized with cyclic voltammetry using different sweep rates, upper reversal potentials, and rotation rates. All experiments were performed at room temperature.

## 3. Results

For solutions saturated with CO(aq), the current before the oxidation peak is close to zero. In this potential region, the platinum surface has a high coverage of CO(ads). Since adsorbed CO and the oxygenating species compete for the same surface sites, the surface is blocked by CO(ads). As the potential increases, the driving force toward PtOH or PtO formation increases as well, and will eventually be sufficient for it to take place on a larger fraction of the surface. Reaction between CO(ads) and PtOH then occurs to form $CO_2$, yielding an increasing current. Two new free platinum sites are also formed by this reaction, leading to more adsorbed OH and thus increased reaction rate. This leads to the steep CO oxidation peak. After the oxidation peak, the oxidation current depends on the rotation rate and decreases with potential up to 1.6 V, Fig. 1. At 1.2-1.3 V, depending on the rotation rate, the current starts to decrease more quickly. At 1.5-1.6 V, the current is almost the same for all rotation rates. On the reverse scan, the current is low for all rotation rates until a small oxidation peak appears at a potential more negative than the forward peak potential. This behavior is well-known from the literature [3, 9, 16, 22, 23, 32–34].

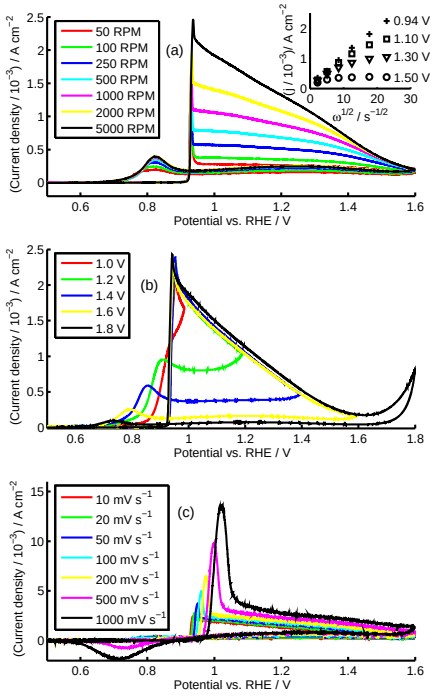


Figure 1: Experimental cyclic voltammograms. (a) varying rotation rates, 10 mV $s^{-1}$, (b) varying reversal potentials, 10 mV $s^{-1}$ and 5000 rpm, (c) varying sweep rates, 5000 rpm. The inset in (a) shows a Levich plot at different potentials.

The inset in Fig. 1a shows Levich plots, $j$ versus $\omega^{1/2}$, at different potentials. Right after the oxidation peak, the line is linear for all rotation rates. With increasing potential, the current deviates from a straight line at higher rotation rates and becomes almost horizontal at 1.5 V. Thus, the reaction is mass-transfer limited right after the peak and becomes reaction limited when the potential increases. This becomes clear at 1.6 V, where the current is no longer affected by the rotation rate.

When the reversal potential increases from 1.0 to 1.8 V, two effects are visible in the cyclic voltammogram, Fig. 1b: 1) the magnitude of the current plateau decreases, and on the reverse sweep the current is approximately constant at the value at the reversal potential, and 2) the reverse scan oxidation peak undergoes a negative shift and the peak height decreases. Thus, the current is deactivated at a lower potential when the reversal potential is increased.

With increasing sweep rate, Fig. 1c, the main oxidation peak grows and shifts toward higher potentials. The oxidation peak becomes broader and less steep. On the negative-going scan, the oxidation peak disappears and a reduction peak appears. The reduction peak grows and shifts toward negative potentials with increasing sweep rate. At the highest sweep rates, the reverse scan becomes quite similar to the reverse scan for cyclic voltammograms in 0.5 M sulfuric acid without CO(g).

## 4. Modelling

Each model adds reaction steps to the basic Langmuir-Hinshelwood mechanism, Eqs. (1) - (3), where CO and OH adsorb on the surface and then react to form $CO_2$.

$$\mathrm{CO(aq)} + \mathrm{Pt} \underset{k_{-1}}{\overset{k_1}{\rightleftarrows}} \mathrm{PtCO(ads)} \tag{1}$$

$$\mathrm{H_2O} + \mathrm{Pt} \underset{k_{-2}}{\overset{k_2}{\rightleftarrows}} \mathrm{PtOH(ads)} + \mathrm{H^+} + \mathrm{e^-} \tag{2}$$

$$\mathrm{PtCO(ads)} + \mathrm{PtOH(ads)} \overset{k_3}{\rightarrow} \mathrm{CO_2} + \mathrm{H^+} + \mathrm{e^-} + 2\mathrm{Pt} \tag{3}$$

Here, the use of PtOH(ads) rather than simply OH(ads) is a reminder of the assumed stoichiometry of one OH per Pt atom. Since linear adsorbed CO dominates at the high coverages and high potentials [35] appropriate for most of our experimental parameter space, it is assumed that CO only adsorbs on the on-top site, and that CO and OH compete for the same sites. The models are constructed as a set of reaction steps (including the above three), which have rates obeying conventional mass-action kinetics. The net rate for each step, $v_j$ (mol cm$^{-2}$ s$^{-1}$) is the forward rate minus the reverse rate, e.g., Eqs. (4) - (6) for the above reactions.

$$v_1 = k_1 c_\mathrm{s} \theta_\mathrm{Pt} - k_{-1} \theta_\mathrm{CO} \tag{4}$$

$$v_2 = k_2 \theta_\mathrm{Pt} \exp\left((1-\beta_2)\, FE/RT\right) - k_{-2} \theta_\mathrm{PtOH} \exp\left(-\beta_2 FE/RT\right) \tag{5}$$

$$v_3 = k_3 \theta_\mathrm{PtCO} \theta_\mathrm{PtOH} \exp\left((1-\beta_3)\, FE/RT\right) \tag{6}$$

Here $c_\mathrm{s}$ is the concentration of CO at the electrode surface. As discussed above, the mass-action assumption for adsorbed species (e.g., $\theta_\mathrm{PtCO}\theta_\mathrm{PtOH}$ in step 3) is the mean-field assumption consistent with fast surface diffusion. All reactions where $CO_2$ is formed as product are assumed to be irreversible.

The effect of adsorbed anions is not included in the models presented here. The usual Tafel-like potential dependence of rate constants is assumed for the charge-transfer reactions.

The net rate of production for each species, $r_i$, is a combination of the rates of each step in which the species is produced or removed, e.g., for model 1, $r_{\mathrm{CO}} = -v_1 - v_5 - v_7$. Free surface sites are treated like adsorbed species. This leads to a set of differential equations describing the time evolution of coverage of each adsorbed species, Eq. (7), where the surface coverages are defined as ratios of the number of adsorbed species to the number of surface atoms on the (unreconstructed) clean Pt surface. The surface concentration of these Pt atoms is $\Gamma_{\mathrm{m}} = 2.28$ nmol cm$^{-2}$. These differential equations are supplemented by a constraint amongst the coverages, which simplifies to Eq. (8) in the models here where all adsorption sites are equivalent and there is one site per Pt. The mass transport flux of CO to/from the surface must be equal to rate of its consumption/production by the reactions, Eq. (9). The RDE convective-diffusive flux at the surface was assumed to be well approximated by its steady-state value, Eq. (10), where $\nu = 0.01$ cm$^2$ s$^{-1}$ is the kinematic viscosity, $D_{\mathrm{CO}} = 5 \times 10^{-5}$ cm$^2$ s$^{-1}$ is the diffusivity, and $c^* = 1$ mM is the bulk concentration of CO. This approximation is justified by the fact that the potential traversed in the characteristic diffusion time, $\delta^2/D_{\mathrm{CO}}$, is no more than 3 mV for any of the results presented here except for the three lowest rotation rates at 10 mV s$^{-1}$, where it is $6 - 30$ mV. The surface concentrations and coverages were calculated by solving the set of differential and algebraic equations (7) - (10) numerically for potential sweep conditions using Maple's Rosenbrock differential/algebraic equation solver. The current density was then found from the net rate of production of electrons, Eq. (11). Unless specified otherwise, all symmetry factors were set equal to 0.5.

$$\Gamma_{\mathrm{m}} \frac{d\theta_i}{dt} = r_i \tag{7}$$

$$\sum_i \theta_i = 1 \tag{8}$$

$$r_{\mathrm{CO}} = J_{\mathrm{CO}} \tag{9}$$

$$J_{\mathrm{CO}} = -D_{\mathrm{CO}} \left( \frac{c^* - c_{\mathrm{s}}}{\delta} \right), \ \delta = 1.61 \nu^{1/6} D_{\mathrm{CO}}^{1/3} \omega^{-1/2} \tag{10}$$

$$j/F = r_{\mathrm{e}} \tag{11}$$

*4.1. Model 1*

$$\mathrm{PtOH(ads)} \underset{k_{-4}}{\overset{k_4}{\rightleftarrows}} \mathrm{PtO_a} + \mathrm{H^+} + \mathrm{e^-} \tag{12}$$

$$\mathrm{PtOH(ads)} + \mathrm{CO(aq)} \underset{k_{-5}}{\overset{k_5}{\rightleftarrows}} \mathrm{PtOH\text{-}CO(ads)} \tag{13}$$

$$\mathrm{PtOH\text{-}CO(ads)} \overset{k_6}{\rightarrow} \mathrm{CO_2} + \mathrm{H^+} + \mathrm{e^-} + \mathrm{Pt} \tag{14}$$

$$\mathrm{PtO_a} + \mathrm{CO(aq)} \underset{k_{-7}}{\overset{k_7}{\rightleftarrows}} \mathrm{PtO_a\text{-}CO(ads)} \tag{15}$$

$$\mathrm{PtO_a\text{-}CO(ads)} \overset{k_8}{\rightarrow} \mathrm{CO_2} + \mathrm{Pt} \tag{16}$$

$$\mathrm{PtO_a} \underset{k_{-9}}{\overset{k_9}{\rightleftarrows}} \mathrm{PtO_b} \tag{17}$$

$$\mathrm{PtO_b} + \mathrm{H^+} + \mathrm{e^-} \overset{k_{10}}{\rightarrow} \mathrm{PtOH(ads)} \tag{18}$$

Model 1 supplements the basic three reactions, Eqs. (1) - (3), with the above seven reactions, Eqs. (12) - (18). The approach in this model is to use only elementary chemical and electrochemical reaction steps to model bulk CO oxidation and platinum oxide formation. The oxide kinetics are treated as though the oxide were composed of the adsorbed species PtOH(ads), $\mathrm{PtO_a}$ and $\mathrm{PtO_b}$, but we avoid the (ads) label for the last two since surface reconstruction is likely on the real surface at potentials where they predominate. Oxidation of platinum to the oxide is assumed to proceed through PtOH to $\mathrm{PtO_a}$ and then to $\mathrm{PtO_b}$. We have argued elsewhere that a Pt(II) species predominates under these conditions [36]. Both PtOH and $\mathrm{PtO_a}$ are allowed to react directly with dissolved CO, but only PtOH reacts with adsorbed CO. $\mathrm{PtO_b}$ is inert towards dissolved CO. The conversion of $\mathrm{PtO_a}$ to $\mathrm{PtO_b}$ on the forward sweep is determined by potential through the reverse rate constant $k_{-9}\exp(-0.18FE/RT)$. On the reverse sweep, $k_{-9} = 0$ and $\mathrm{PtO_b}$ is reduced directly to PtOH without proceeding through $\mathrm{PtO_a}$.

*4.2. Model 2*

*4.2.1. Oxide equation*

The second model replaces the reactions involving platinum oxide species $\mathrm{PtO_a}$ and $\mathrm{PtO_b}$ with an empirical equation describing the current due to platinum oxide growth and reduction in cyclic voltammograms for platinum

in sulfuric acid, Eq. (19). This equation is based on the platinum oxide growth equation developed by Heyd and Harrington [37]. The first term in Eq. (19) is the oxidation current due to platinum oxide growth. This term describes the rate of the rate determining step, assumed to be the place exchange process where the Pt atom leaves the platinum lattice and bonds to oxygen. The second term describes reduction of the platinum oxide, in a way similar to that used by Darling and Meyers [38]. This term is based on a Tafel factor for a reduction reaction multiplied with an empirically determined correction factor to obtain the right behavior of the reduction peak with respect to sweep rate and upper reversal potential.

$$v_6 = (1-\theta_{\mathrm{PtCO}})^2 k_6 \exp(cE) \exp(-b\Theta) \tag{19}$$

$$- k_{-6}\Theta \exp\left(-\frac{\beta_6 FE}{RT}\right) k_{E_{\mathrm{up}}} v^{0.8198} \times \exp\left(-\frac{(-0.279+0.18E_{\mathrm{up}})FE}{RT}\right) \tag{20}$$

where the rate constant $k_6$ determines the onset potential for platinum oxidation, $c$ determines the steepness of the current rise, $b$ determines the current plateau, $v$ is the sweep rate in V $\mathrm{s}^{-1}$, $\Theta$ is the time-dependent "coverage" of electrons (the number of electrons transferred to form platinum oxide per platinum site) and $E_{\mathrm{up}}$ is the upper reversal potential in V. The parameter $k_{E_{\mathrm{up}}}$ is given by

$$k_{E_{\mathrm{up}}} = \begin{cases} 1.734E_{\mathrm{up}} - 1.8179, & E_{\mathrm{up}} \geq 1.146 \\ 0.575E_{\mathrm{up}} - 0.4895, & E_{\mathrm{up}} < 1.146 \end{cases} \tag{21}$$

The model distinguishes the coverage based on counting electrons, $\Theta$, from the coverage based on counting occupied Pt sites, $\theta_{\mathrm{PtO}}$, to allow for multilayer growth before a monolayer of sites is occupied. We find that

$$\theta_{\mathrm{PtO}} = \frac{1}{2}\Theta H(1.5-\Theta) + (1-5.02\exp(-2\Theta))(1-H(1.5-\Theta)) \tag{22}$$

where $H$ is the Heaviside step function. The change of behaviour around 1.5 $\mathrm{e}^-$/Pt is consistent with the observation by X-ray reflectivity that the surface reconstruction begins at about 1.7 $\mathrm{e}^-$/Pt [39]. The coverage $\Theta$ was used in the differential equation for PtO, Eq. (7), but $\theta_{\mathrm{PtO}}$ was used in Eq. (8). The parameters in Eqs. (19) - (21) were determined by fitting

to experimental cyclic voltammograms of platinum in 0.5 M sulfuric acid, giving: $k_6 = 5 \times 10^{-19}$ mol cm$^{-2}$ s$^{-1}$, $k_{-6} = 8.12 \times 10^{-3}$ mol cm$^{-2}$ s$^{-1}$, $.c = 25$ V$^{-1}$, $b = 9$, $\beta_6 = 0.43$. The prefactor $(1 - \theta_{\mathrm{PtCO}})^2$ was then added to model the inhibition of the initial oxidation by strongly-bound adsorbed CO.

*4.2.2. Model description*

The basic reactions (1)-(3) are supplemented by

$$\mathrm{PtOH(ads)} + \mathrm{CO(aq)} \underset{k_{-4}}{\overset{k_4}{\rightleftarrows}} \mathrm{PtOH\text{-}CO(ads)} \tag{23}$$

$$\mathrm{PtOH\text{-}CO(ads)} \xrightarrow{k_5} \mathrm{CO_2} + \mathrm{H^+} + \mathrm{e^-} + \mathrm{Pt} \tag{24}$$

$$\mathrm{PtOH(ads)} \underset{k_{-6}}{\overset{k_6}{\rightleftarrows}} \mathrm{PtO} + \mathrm{H^+} + \mathrm{e^-} \tag{25}$$

with step 6 being the formation and reduction of the oxide according to Eqs. (19) and (21). As in model 1, PtOH is allowed to react directly with dissolved CO but, in contrast, PtO is here inert and does not react with dissolved CO. The model was fitted to the experimental results by adjusting the rate constants. The forward rate constants $k_1$ and $k_2$ for reactions (1) and (2) were given separate values for the forward and reverse scan directions. The former shifts to a lower value for the reverse scan and the latter shifts to a higher value that depends on the upper limit potential. Thus, the adsorption of OH is stronger relative to CO adsorption on the reverse scan compared with the forward scan.

*4.3. Results*

*4.3.1. Model 1*

The following rate constants (given at 0 V vs RHE) gave good general agreement between the modelled cyclic voltammograms, Fig. 2, and the experimental ones, Fig. 1: $k_1 = 2.3 \times 10^{-3}$, $k_5 = 2.7 \times 10^{-2}$, $k_7 = 2.3 \times 10^{-2}$ cm s$^{-1}$; $k_{-1} = 2.3 \times 10^{-17}$, $k_2 = 1.8 \times 10^{-15}$, $k_{-2} = 2.3 \times 10^{-4}$, $k_3 = 1.1 \times 10^{-16}$, $k_4 = 2.3 \times 10^{-18}$, $k_{-4} = 2.3 \times 10^{-13}$, $k_{-5} = 2.3 \times 10^{-9}$, $k_6 = 2.3 \times 10^{-13}$, $k_{-7} = 2.3 \times 10^{-8}$, $k_8 = 1.1 \times 10^{-7}$, $k_9 = 4.6 \times 10^{-8}$, $k_{-9} = 1.8 \times 10^{-4}$, $k_{10} = 6.8 \times 10^{-3}$ mol cm$^{-2}$ s$^{-1}$. The initial conditions were $\theta_{\mathrm{PtCO}} = 0.95$, $\theta_{\mathrm{PtOH}} = 0$ and $c = c^*$ at $E = 0.5$ V vs RHE. On the forward sweep there is a sharp CO oxidation peak followed by a gradual current decrease as the

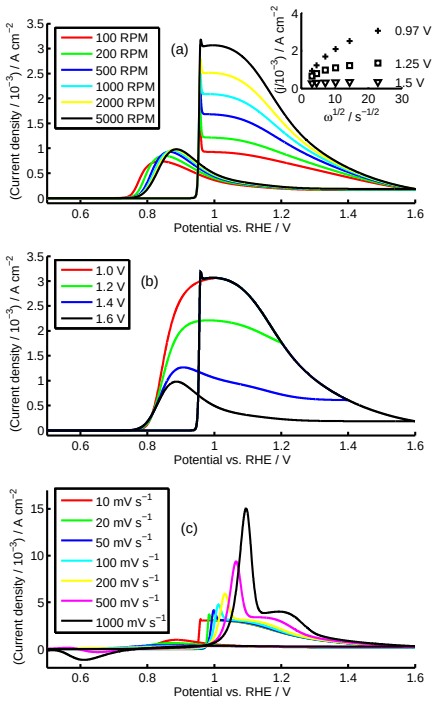


Figure 2: Modelled cyclic voltammograms for model 1. (a) varying rotation rate, 10 mV $s^{-1}$, (b) varying reversal potential, 10 mV $s^{-1}$ and 5000 rpm, (c) varying sweep rate, 5000 rpm. The inset in (a) is a Levich plot at different potentials.

potential increases. On the reverse scan, there is an oxidation peak located at a lower potential than the positive-going scan peak. As the rotation rate increases, both the main oxidation peak height and the current after the peak increase.

At the start of the positive-going scan, the coverage of adsorbed CO is high. This blocks the surface until the potential is high enough for OH to adsorb via reaction 2. Oxidation of adsorbed CO through reaction 3 is now possible, leading to the sharp oxidation peak. Right after the peak, the surface is blocked by oxygen-containing species. CO can no longer adsorb and reaction 3 stops. CO oxidation now proceeds via reactions 5 to 8. As the potential increases, PtOH is converted to $PtO_a$, both being active towards CO oxidation, and $PtO_a$ is converted to $PtO_b$, which is passive towards CO oxidation. The latter conversion leads to fewer active sites for CO oxidation and reduces the reaction rate. On the negative-going scan, no more $PtO_a$ is

converted to $PtO_b$. The amount of $PtO_a$ determines the rate of CO oxidation. Thus, the current is constant until approximately 1.2 V, where reduction of $PtO_b$ to PtOH (reaction 10) commences. As more PtOH is formed, from reactions 2 and 10, the current increases and forms the reverse scan oxidation peak. After this peak, adsorption of OH is slower than CO adsorption, leading to an increasing CO(ads) coverage. Eventually, the surface will again be blocked by adsorbed CO.

Changing the reversal potential greatly affects the reverse scan, Fig. 2b. When decreasing the reversal potential, the amount of active oxygen-containing species is higher at the beginning of the negative-going scan. Thus, the current early in the reverse scan increases with decreasing reversal potential. In addition, the peak potential shifts slightly toward higher potentials and the peak height increases. The current deactivation after the peak remains at the same potential. During the oxidation peak the main reactions are reactions 2, 5, and 6. The deactivation is caused by the rate of PtOH formation becoming slower than CO adsorption rate.

Levich plots for different potentials are shown in the inset in Fig. 2a. For all potentials, the plots deviate from linear behavior in the high rotation rate end, and the deviation starts at a lower rotation rate as the potential increases. Thus, the significance of mass-transfer decreases as the potential increases.

The differences between the modelling results and the experimental results become apparent in the voltammograms with varying sweep rates, Fig. 2c. Here, another oxidation peak appears right after the main oxidation peak at high sweep rates and the reverse scan peak shifts too fast to negative potentials.

*4.3.2. Model 2*

The first approach with model 2 was to keep all the rate constants constant during the forward and reverse scans: $k_1 = 0.18, k_4 = 2.3 \times 10^{-2}$ cm $s^{-1}$; $k_{-1} = 1.8 \times 10^{-11}$, $k_2 = 1.1 \times 10^{-13}$, $k_{-2} = 23$, $k_3 = 2.3 \times 10^{-16}$, $k_{-4} = 1.1 \times 10^{-14}$, $k_5 = 6.8 \times 10^{-15}$ mol $cm^{-2}$ $s^{-1}$. The initial conditions were $\theta_{PtCO} = 0.9999$, $\theta_{PtOH} = 0$, $\Theta = 0$ and $c = c^*$ at $E = 0.5$ V vs RHE. The resulting cyclic voltammogram and the coverages of each surface species are shown in Fig. 3. The forward sweep in this cyclic voltammogram shows the same features as in the experimental cyclic voltammogram. At low potentials, the surface coverage of CO is close to 1 and the surface is completely blocked by adsorbed CO. The current in this region is thus zero. Around 0.93

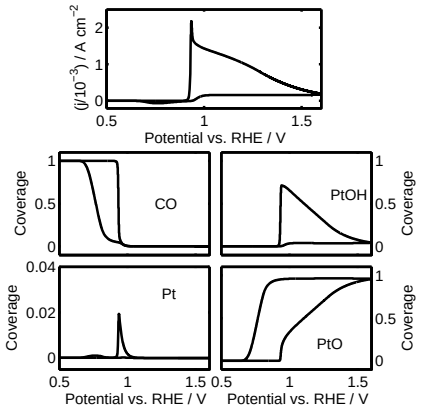


Figure 3: Results from the first approach of model 2. (Top) Cyclic voltammogram. (Bottom) Surface coverages of the different adsorbed species during cyclic voltammetry. The sweep rate is 10 mV $s^{-1}$.

V, OH starts to adsorb on the surface. Oxidation of CO to $CO_2$ is now possible, via reactions 3 - 5, resulting in a very steep CO oxidation peak. During the rising part of the peak, the surface changes from a high coverage of adsorbed CO to a high coverage of adsorbed OH. After the peak, the current decreases slowly with increasing potential. Due to the potential dependence of reaction 2, adsorption of OH dominates over adsorption of CO. Thus, CO will not adsorb in this potential region and oxidation of CO proceeds only via reactions 4 and 5. The former reaction, a chemical reaction step, is rate limiting, leading to a current proportional to the OH coverage. As more PtOH is converted to PtO with increasing potential, the current decreases. As can be seen in Fig. 3, no PtO is formed before CO oxidation commences. The coverage of PtO increases rapidly right after the CO oxidation peak and continues to increase slowly with increasing potential.

On the upper half of the negative-going scan, the coverages and current remain constant at their values at the upper reversal potential. As with the upper part of the forward sweep, CO oxidation proceeds only via reactions 4 and 5 with the former as rate determining step. As the potential decreases, the rate of OH adsorption (reaction 2) also decreases and will eventually become the rate determining step. At this point, the coverage of PtOH starts to decrease and the CO coverage increases. At more negative potentials, a small reduction peak caused by platinum oxide reduction is visible.

The next approach was to allow some of the rate constants to change

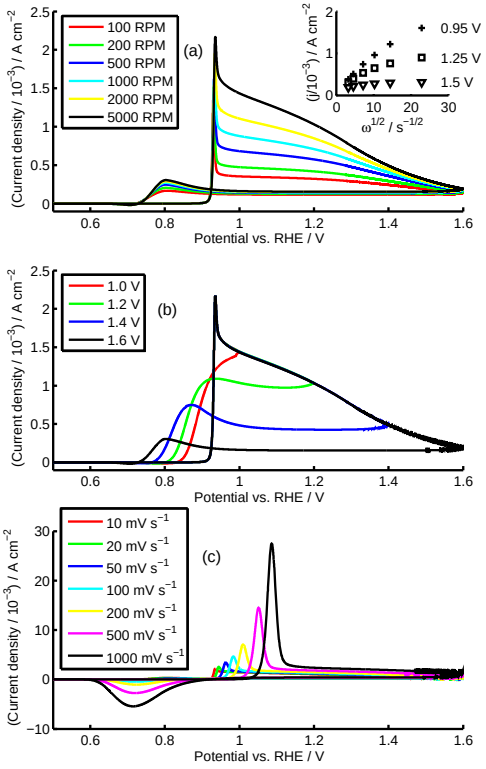


Figure 4: Modelled cyclic voltammograms for model 2. (a) varying rotation rates, 10 mV $s^{-1}$, (b) varying reversal potentials, 10 mV $s^{-1}$ and 5000 rpm, (c) varying sweep rates, 5000 rpm. The inset in (a) is a Levich plot at different potentials.

values on the reverse scan. Specifically, $k_1$ was divided by 100, and $k_2$ was multiplied by 0.1 at 1.0 V reversal potential, by 0.4 at 1.2 V, by 2.0 at 1.4 V and by 10 at 1.6 V. With this approach, the effects of varying experimental parameters, such as rotation rate, sweep rate and upper reversal potential, were studied. For the case of varying rotation rate, the resulting cyclic voltammograms are very similar to the experimental results, Fig. 4a. The current response for the forward sweep is the same as described above. In the potential region after the CO oxidation peak, the current response is strongly influenced by rotation rate. Faster rotation leads to higher currents. The Levich plots (inset in Fig. 4a), are straight lines for potentials right after the CO oxidation peak, but deviate from straight lines at higher rotation rates later in the potential sweep. Thus, right after the oxidation peak,

the current is limited by solution diffusion. For the slowest rotation rates, this is true up to approximately 1.2 V. Between the oxidation peak and the reversal potential, the current decreases almost linearly with potential, but at approximately 1.25 V, the current starts to decrease more quickly. At the reversal potential, 1.6 V, the current is almost independent of rotation rate. On the reverse scan, the current remains approximately constant until the oxidation peak. The height of this peak increases slightly with rotation rate, but the peak potential is unaffected by rotation rate.

The reverse scan is strongly affected by variation of the upper reversal potential, Fig. 4b. As the reversal potential is decreased from 1.6 V, the reverse scan oxidation peak shifts toward more positive potentials, the peak height increases, and the current after the peak deactivates at higher potentials. When the sweep is reversed at 1.0 V, the reverse scan oxidation peak disappears. The current deactivates almost immediately. After deactivation, the current remains close to zero for the rest of the scan.

As the sweep rate is increased, the forward oxidation peak shifts positively and the peak height increases, Fig. 4c. The peak is much less steep at higher sweep rates. The current after the oxidation peak changes from being dominated by CO oxidation (reactions 2, 4, and 5) to being affected significantly by platinum oxide formation (reaction 6) in addition to CO oxidation. On the reverse scan, the oxidation peak evolves into a reduction peak as the sweep rate increases.

## 5. Discussion

### *5.1. Model reactions*

In both models, PtOH, formed by electrochemical adsorption of $H_2O$, is the initial oxygen-donor species. As the potential increases, the rate of PtOH formation increases relative to the CO adsorption rate. At potentials higher than the oxidation peak, the rate of PtOH formation is significantly higher than the rate of CO adsorption, and PtOH will dominate over adsorbed CO on the surface. When PtOH starts to form, some PtOH is further oxidized to PtO. The surface is now blocked by an oxygen-containing species, PtOH or PtO. Thus, CO ceases to adsorb on the surface. The experimental results clearly show an oxidation current in this potential region. This suggests that CO may be oxidized through a mechanism not involving adsorbed CO. A direct reaction between PtOH and dissolved CO was proposed in both models. This pathway consists of two reaction steps: 1) adsorption of CO

on PtOH, a chemical reaction step, and 2) oxidation of the adsorbed species, PtOH-CO to $CO_2$, an electrochemical reaction step. The former reaction step is rate limiting.

In model 1, most PtOH is converted to PtO around 1.2 V. The experimental cyclic voltammogram still shows an oxidation current at this potential. Thus, another direct reaction, between PtO and CO(aq), is added. This reaction is considered to consist of two reaction steps: 1) adsorption of CO on PtO and 2) reaction of PtO-CO to $CO_2$, with step 1 as rate limiting. In order to obtain the passivation with increasing potential, the platinum oxide was divided into two types, one active, $PtO_a$, and one passive, $PtO_b$.

The direct reaction between PtO and CO(aq) is not included in model 2. Here, PtOH is considered active towards CO oxidation while PtO is considered to be inert, and the oxidation from PtOH to PtO is governed by the oxide equation. The platinum oxide formation mechanism now better describes the reconstructed surface than an adsorption model like model 1.

On the negative-going scan, the onset of the oxidation peak appears at too high a potential for model 1, in comparison with the experimental results. In this model, $CO_2$ is formed through a direct reaction between dissolved CO and PtO, reactions 7 and 8. These are chemical reactions and the rates do not depend on the potential. As the potential decreases, the platinum oxide growth rate decreases and will, at some point, be lower than those direct reactions. Thus, the coverage of PtO decreases before oxide reduction commences, Fig. 5. This creates active sites for further CO oxidation. In the experimental results, the onset of the reverse scan peak is approximately at the same potential as the onset of PtO reduction. This suggests that PtO does not react directly with dissolved CO.

*5.2. Effect of rate parameters in model 2*

The different features in the experimental cyclic voltammogram put different constraints on the values of the rate parameters. To obtain the steep CO oxidation peak in the modelling, a CO coverage close to unity is necessary. Otherwise, adsorption of OH will start at lower potentials and, since reactions 2 and 3 are slower here, the resulting oxidation peak will not be as steep as in the experiments. Especially the early current rise will be less steep. Thus, the ratio $k_1/k_{-1}$ must be as high as possible. When modelling the cyclic voltammograms for increasing sweep rates, this ratio has to be lower to obtain the correct peak behavior. Too high a ratio has two consequences when increasing the sweep rate: 1) the peak current increases too

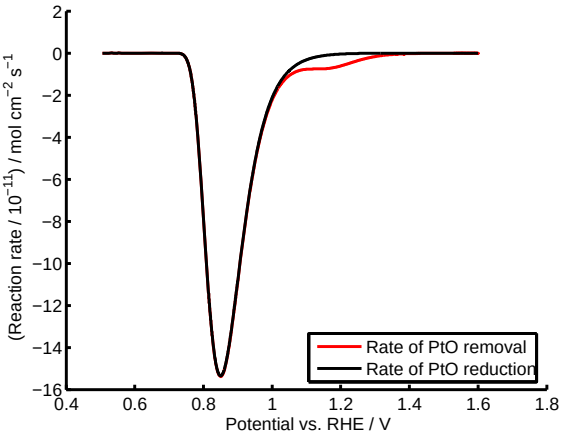


Figure 5: The rate of platinum oxide removal and rate of platinum oxide reduction from model 1 plotted as a function of potential.

much, and 2) the positive shift of the peak is too large.

For the positive scan, the ratio $k_1/k_2$ is important for the location of the oxidation peak. Increasing the ratio leads to a negative shift and reduced height and steepness for the peak, and vice versa for decreasing this ratio. On the reverse scan, this ratio determines whether the oxidation peak will appear or not. If the value is too high, the peak will disappear, as in Fig. 3. The constraints on $k_1/k_2$ are different on the forward and the reverse scans. The former demands higher values than the latter. No good compromise that gives both accepteable positive and negative scans was found. In the model, this problem was arbitrarily solved by allowing different values on the positive and negative scans for some of the rate constants. Thus, $k_1$ is allowed to decrease and $k_2$ is allowed to increase on the reverse scan. The physical interpretation of this must be that the presence of PtOH/PtO on the surface reduces the CO adsorption energy and enhances the PtOH formation rate.

On the reverse scan, the potential at which the current deactivates after the peak shifts to lower potentials with decreasing reversal potential. As noted in section 4.3.2, this is determined by the rate of OH adsorption, since the current deactivates when OH no longer adsorbs on the surface. Thus, the rate constant, $k_2$, has to increase with increasing reversal potential. When the reversal potential is higher, more PtO has been formed and more PtO is present on the negative-going scan. This suggests that the adsorption of OH is enhanced by the presence of PtO on the surface.

*5.3. Oxidation of CO on the reverse scan*

The reduction of Pt oxide on the reverse scan exposes free sites on which CO adsorption can occur. The rate of adsorption of CO and the adsorption site depends strongly on many variables such as the adsorption potential and time, and CO solution concentration. The sweep conditions here are not those usually found in such adsorption studies, so it is hard to predict the state that CO will be in after oxide reduction. However, we may assume the coverage is relatively low, and concentration dependence studies by several groups [13, 40–42] show that an open adsorbed CO structure that is easily oxidized forms at low CO solution concentrations. This is consistent with CO oxidation at lower potentials on the reverse sweep after oxide reduction (low CO coverage) than on the forward sweep (high coverage). The potential range for the reverse scan oxidation peak is similar to the potential range where CO is oxidized at low coverages.

Han and Ceder [43] found, by DFT calculations, that coadsorption of CO with O or OH on Pt weakens the Pt-CO bond through a largely strain mediated interaction. Thus, it is quite likely that the adsorption energies for the first half of the reverse scan will be different than for the first half of the forward scan. Adsorption on the free platinum sites formed during reduction of platinum oxide on the reverse scan is quite different from adsorption on free platinum sites formed during CO oxidation on the forward sweep. The difference is that adsorption is on platinum sites surrounded by adsorbed CO on the forward scan, but on platinum sites surrounded by platinum oxide on reverse scan. This major change of surface composition will likely have a significant consequence on the adsorption rates of CO and OH.

In the voltammograms with varying reversal potentials, Fig. 4b, the surface is mostly covered by an oxygen-containing species at the reversal potential. The key difference between the different potential limits is the distribution between PtOH (active) and PtO (passive). As the reversal potential is increased, more PtO is formed, and, on the reverse scan, CO oxidation is possible at a lower potential. This indicates that the presence of PtO enhances the oxidation of CO in the potential region where the PtO is reduced.

*5.4. Nature of the oxide*

It is evident that the smaller amount of CO oxidation at higher potentials is due to the formation of non-reactive oxide at the higher potentials. Model 1 explains this by transformation from an active species $PtO_a$ to an inactive

species $PtO_b$. This model is simplistic but suggests that a change in structure of the oxide is responsible for the reduced reactivity. However, better results were obtained by the empirical oxide growth equation used in model 2. This equation was optimized for results in the absence of CO, and is validated by its success in the presence of CO. The key reason for the decreased reactivity in model 2 at higher potentials is not an intrinsic change in the structure of the oxide, but a decrease in the area free of unreactive oxide, where reaction between adsorbed PtOH and CO is possible.

The empirical equation used here is based on a direct logarithmic growth law for constant potential conditions adapted to cyclic voltammetry [37]. This law, the inverse logarithmic law, or some combination of the two, can give similar fits to experimental constant-potential oxide growth data. The interpretation is variously given in terms of field-driven dipole flipping by Conway [44], dipole flipping and also cation injection into a thin-film (Mott-Cabrera model) by Jerkiewicz [45, 46], or cation injection into a thin film (point-defect model) by Macdonald [47]. A debate between these models is outside the scope of this paper, and it might seem that more recent experimental data should have resolved this issue. However, new methods that give good structural information e.g., X-ray methods often require long acquisition times and fail to give kinetic information, though some time resolved X-ray data partly supports the direct logarithmic law [48, 49]. Likewise, the presence of H is not directly determined in most methods, and the transition from PtOH to PtO is not well established. For example, electrochemical quartz-crystal microbalance results have been used to support this assertion [9] or deny it [50]. The present results could likely be adapted to other assumptions about the molecular-level identities of the oxide species, but the way in which the reactivity towards CO oxidation decreases at higher potentials likely has significance independently of these assumptions.

## 6. Conclusions

Two different models based on elementary chemical and electrochemical reaction steps were produced in order to model the current-potential characteristics for CO oxidation on polycrystalline platinum in CO-saturated sulfuric acid well into the platinum oxide potential range. Both models reproduce the main features of the experimental voltammograms. One of the models utilizes an empirical equation describing the reaction rate for platinum oxide formation and reduction during cyclic voltammetry.

The modelling leads to the following conclusions:

1. At potentials higher than the main oxidation peak, CO oxidizes via a direct reaction between PtOH and dissolved CO. The surface in this potential region is blocked by a high coverage of PtOH, and CO can not adsorb.
2. On the negative-going scan, CO adsorption is weaker than on the positive-going scan. Here, the surface has a high coverage of PtOH and PtO.
3. There is no reaction between platinum oxide and CO, either adsorbed or in solution.
4. The formation rate of PtOH increases as the amount of platinum oxide present on the surface during the negative-going scan increases.

## Acknowledgments

The Natural Sciences and Engineering Research Council of Canada, University of Victoria, and Norwegian University of Science and Technology (NTNU) are gratefully acknowledged for financial support.

## References

[1] R. Parsons, T. VanderNoot, J. Electroanal. Chem. 257 (1988) 9.

[2] B. Beden, C. Lamy, N. R. de Tacconi, A. J. Arvia, Electrochim. Acta 35 (1990) 691.

[3] K. J. J. Mayrhofer, M. Arenz, B. B. Blizanac, V. Stamenkovic, P. N. Ross, N. M. Marković, Electrochim. Acta 50 (2005) 5144.

[4] M. T. M. Koper, S. C. S. Lai, E. Herrero, in: M. T. M. Koper (Ed.), Fuel Cell Catalysis: A Surface Science Approach, Wiley & Sons, Chichester, 2009, pp. 159–207.

[5] T. D. Jarvi, E. M. Stuve, in: J. Lipkowski, P. N. Ross (Eds.), Electrocatalysis, Wiley-VCH, New York, 1998, pp. 75–154.

[6] N. M. Marković, P. N. Ross Jr, Surf. Sci. Rep. 45 (2002) 117.

[7] K. J. J. Mayrhofer, M. Hanzlik, M. Arenz, Electrochim. Acta 54 (2009) 5018.

[8] M. S. Rau, M. R. Gennero de Chialvo, A. Chialvo, J. Solid State Electrochem. (2012). In press, doi:10.1007/s10008-011-1597-z.

[9] G. Stalnionis, L. Tamasauskaite Tamasiunaite, V. Pautieniene, Z. Jusys, J. Electroanal. Chem. 590 (2006) 198.

[10] M. Bergelin, E. Herrero, J. M. Feliu, M. Wasberg, J. Electroanal. Chem. 467 (1999) 74.

[11] Z. Jusys, J. Kaiser, R. J. Behm, Phys. Chem. Chem. Phys. 3 (2001) 4650.

[12] C. Saravanan, N. M. Marković, M. Head Gordon, P. N. Ross, J. Chem. Phys. 114 (2001) 6404.

[13] J. M. Orts, E. Louis, L. M. Sander, J. M. Feliu, A. Aldaz, J. Clavilier, Surf. Sci. 416 (1998) 371.

[14] J. M. Orts, E. Louis, L. M. Sander, J. Clavilier, Electrochim. Acta 44 (1998) 1221.

[15] C. A. Angelucci, E. Herrero, J. M. Feliu, J. Phys. Chem. C 114 (2010) 14154.

[16] M. T. M. Koper, T. J. Schmidt, N. M. Marković, P. N. Ross, J. Phys. Chem. B 105 (2001) 8381.

[17] R. Nieminen, A. P. J. Jansen, Appl. Catal., A 160 (1997) 99.

[18] A. M. de Becdelièvre, J. de Becdelièvre, J. Clavilier, J. Electroanal. Chem. 294 (1990) 97.

[19] M. T. M. Koper, A. P. J. Jansen, R. A. van Santen, J. J. Lukkien, P. A. J. Hilbers, J. Chem. Phys. 109 (1998) 6051.

[20] T. H. M. Housmans, C. G. M. Hermse, M. T. M. Koper, J. Electroanal. Chem. 607 (2007) 69.

[21] O. V. Cherstiouk, P. A. Simonov, V. I. Zaikovskii, E. R. Savinova, J. Electroanal. Chem. 554-555 (2003) 241.

[22] H. A. Gasteiger, N. M. Marković, J. P. N. Ross, J. Phys. Chem. 99 (1995) 8290.

[23] S. Malkhandi, A. Bonnefont, K. Krischer, Surf. Sci. 603 (2009) 1646.

[24] D. Zhang, O. Deutschmann, Y. E. Seidel, R. J. Behm, J. Phys. Chem. C 115 (2011) 468.

[25] C. Saravanan, M. T. M. Koper, N. M. Marković, M. Head Gordon, P. N. Ross, Phys. Chem. Chem. Phys. 4 (2002) 2660.

[26] A. Bonnefont, H. Varela, K. Krischer, J. Phys. Chem. B 109 (2005) 3408.

[27] A. Bonnefont, R. Morschl, P. Bauer, K. Krischer, Electrochim. Acta 55 (2009) 410.

[28] D. C. Azevedo, A. L. N. Pinheiro, R. M. Torresi, E. R. Gonzalez, J. Electroanal. Chem 532 (2002) 43.

[29] M. J. Janik, C. D. Taylor, M. Neurock, Top. Catal. 46 (2007) 306.

[30] M. J. Janik, M. Neurock, Electrochim. Acta 52 (2007) 5517.

[31] J. Narayanasamy, A. B. Anderson, J. Electroanal. Chem. 554-555 (2003) 35.

[32] C. McCallum, D. Pletcher, J. Electroanal. Chem. 70 (1976) 277.

[33] M. Heinen, Y. X. Chen, Z. Jusys, R. J. Behm., Electrochim. Acta 52 (2007) 5634.

[34] N. M. Marković, T. J. Schmidt, B. N. Grgur, H. A. Gasteiger, P. N. Ross, J. Phys. Chem. B 103 (1999) 8568.

[35] M. Nakamura, H. Ogasawara, J. Inukai, M. Ito, Surf. Sci. 283 (1993) 248.

[36] M. E. van der Geest, N. J. Dangerfield, D. A. Harrington, J. Electroanal. Chem. 420 (1997) 89.

[37] D. V. Heyd, D. A. Harrington, J. Electroanal. Chem. 335 (1992) 199.

[38] R. M. Darling, J. P. Meyers, J. Electrochem. Soc. 150 (2003) A1523.

[39] H. You, D. J. Zurawski, Z. Nagy, R. M. Yonco, J. Chem. Phys. 100 (1994) 4699.

[40] M. Watanabe, S. Motoo, J. Electroanal. Chem. 206 (1986) 197.

[41] J. M. Feliu, J. M. Orts, A. Fernandez Vega, A. Aldaz, J. Electroanal. Chem. 296 (1990) 191.

[42] J. A. Caram, C. Gutiérrez, J. Electroanal. Chem. 346 (1993) 451.

[43] B. C. Han, G. Ceder, Phys. Rev. B: Condens. Matter Mater. Phys. 74 (2006) 205418.

[44] B. E. Conway, B. Barnett, H. Angerstein Kozlowska, B. V. Tilak, J. Chem. Phys. 93 (1990) 8361.

[45] M. Alsabet, M. Grden, G. Jerkiewicz, J. Electroanal. Chem. 589 (2006) 120.

[46] G. Jerkiewicz, M. Alsabet, M. Grden, H. Varela, G. Tremiliosi Filho, J. Electroanal. Chem. 625 (2009) 172.

[47] A. Sun, J. Franc, D. D. Macdonald, J. Electrochem. Soc. 153 (2006) B260.

[48] H. Imai, K. Izumi, M. Matsumoto, Y. Kubo, K. Kato, Y. Imai, J. Am. Chem. Soc. 131 (2009) 6293.

[49] P. Allen, S. Conradson, M. Wilson, S. Gottesfeld, I. Raistrick, J. Valerio, M. Lovato, J. Electroanal. Chemistry 384 (1995) 99.

[50] G. Jerkiewicz, G. Vatankhah, J. Lessard, M. P. Soriaga, Y.-S. Park, Electrochim. Acta 49 (2004) 1451.